High-resolution spectroscopy of the impurity-induced $Q_3(0)$ transition of solid parahydrogen

Robert M. Dickson,* Takamasa Momose,† Teresa J. Byers,‡ and Takeshi Oka
Department of Chemistry and Department of Astronomy and Astrophysics, The University of Chicago, Chicago, Illinois 60637
(Received 22 July 1996; revised manuscript received 1 August 1997)

Due to the increased localization and long lifetime of the $Q_3(0)$ ($v=3\leftarrow 0$, $J=0\leftarrow 0$) excitation, a series of 17 sharp spectral features has been observed and completely assigned to transitions between specific quantum states of the orthohydrogen/parahydrogen pair. Observed under high resolution between 11 758 and 11 759 cm^{-1}, the ten strongest features are due to crystalline nearest-neighbor pairs of $J=0$ H_2 and $J=1$ H_2 that are undergoing and inducing the transition, respectively, while seven additional features arise from next-nearest-neighbor pairs and farther away neighbor interactions. This study gives a direct measurement of the crystal-field splitting for $J=1$ H_2 in otherwise pure para-H_2 crystals. The measured crystal-field splitting, $\Delta = E(M=\pm 1)-E(M=0)$, is 0.0071 ± 0.0002 cm^{-1}. The excited-state crystalline-field and pair splittings are also directly observed and analyzed. [S0163-1829(98)05301-6]

I. INTRODUCTION

The spectroscopy of electric dipole-forbidden transitions allows a glimpse of underlying fundamental intermolecular and intramolecular processes. In the gas phase, for example, weak collision-induced transitions are observed in which the intermolecular interactions causing the transition are both random and transient. These effects yield a statistical average of the different relative velocities and impact parameters of individual molecules, thus broadening the observed transitions. In a solid environment, however, the molecules are held in place, thus allowing long-term intermolecular interactions. Due to long interaction times and small amplitude molecular motion (much shorter than the wavelength), neither pressure nor Doppler broadening effects arise. Resulting from its weak intermolecular interactions, solid parahydrogen acts in many ways as a high-density ideal gas with limited translational motion and thus allows the observation of very high-resolution spectra. Because the pure vibrational transitions $Q_v(0)$ ($v=v\leftarrow 0, J=0\leftarrow 0$) of hydrogen molecules become infrared-active only upon interaction with other molecules, they provide an excellent probe to study intermolecular interactions. The solid parahydrogenic environment provides a medium that can yield much more detailed and accurate information on intermolecular interactions than gas phase molecular processes have provided.

The pressure-induced vibrational spectrum of hydrogen was first recorded in 1949;[1] these absorptions result from the multipole moment of one molecule inducing a dipole in its collision partner, thus facilitating the absorption of radiation. Analogously, absorptions can also be induced in an isolated molecule by applying an external electric field. This field produces a polarization in the direction of the field allowing the molecule to absorb infrared radiation. As Condon showed, this field-induced transition may be considered as Raman spectroscopy with the frequency of the pump beam tending to zero.[2] In the solid state, molecules are generally so close together that their interactions strongly perturb the transition frequencies of their neighbors. Solid parahydrogen, on the other hand, with its weak intermolecular interactions provides the unique opportunity to have molecules in very close proximity while maintaining the integrity of the rotational and vibrational quantum numbers.[3,4] Upon application of an electric field, Kerr *et al.* have observed very narrow vibrational spectral linewidths in solid parahydrogen, illustrating the purity of the hydrogenic quantum states.[5]

The hexagonal close packed (hcp) crystalline environment of solid p-H_2 provides an anisotropic environment that often results in the observation of strongly polarization-dependent intensities with the electric field of incident radiation parallel and perpendicular to the unique crystalline axis. These polarization dependences have been instrumental in the understanding and the assignment of these transitions. The interactions in solid p-H_2 are greatly simplified by the large rotational constant of hydrogen; the only populated rotational energy levels in the zero pressure solid are $J=0$ (para-H_2) and $J=1$ (ortho-H_2). The $J=0$ state is spherically symmetric; thus, no averaged multipole moments exist. The $J=1$ level, however, exhibits an averaged quadrupole moment that strongly interacts with its neighbors. Since averaged multipole moments are not present in pure parahydrogen crystals, isotropic and anisotropic dispersion forces are the main intermolecular interactions and thus provide the major binding energy of the crystal. These energies, with a R^{-n} ($n\geqslant 6$) distance dependence, are small, but are one to two orders of magnitude stronger than the next strongest interactions: the induction and the second-order electric quadrupole-quadrupole interactions. As a result of the weak intermolecular interactions and very narrow lines previously observed in solid parahydrogen, one might expect to be able to study in detail the interactions that make these transitions infrared active. Even the small energy differences caused by the relative orientations of molecules may be studied. Each molecule in the hcp lattice has two distinct types of nearest neighbors, in plane (ip) and out of plane (op); due to their different angular orientations relative to the crystalline axis, transitions due to ip and op pairs occur at slightly different frequencies.

The presence of an impurity orthohydrogen molecule is necessary for the $Q_v(0)$ absorptions to occur. This is in contrast to the cases of S ($\Delta J=2$), U ($\Delta J=4$), and W ($\Delta J=6$) transitions[6–12] that do not require the average electric

field of an impurity. In these transitions the instantaneous electric field due to the 2^L pole of p-H_2 (with $L=2,4,6$) induces instantaneous dipole moments in the surrounding molecules that cause these transitions. This mechanism does not work for the $Q_v(0)$ transitions since the neutral H_2 molecule does not possess an $L=0$ monopole. Thus, in a pure parahydrogen lattice, the $Q_v(0)$ transitions are rigorously forbidden. Upon introducing an impurity (e.g., orthohydrogen) into the parahydrogen lattice, however, the average quadrupolar field of the impurity can induce dipoles in the surrounding parahydrogen molecules, thus allowing absorption to occur via a simultaneous transition in which the $J=0$ molecule absorbs one quantum of vibrational energy in the field of the neighboring $J=1$ molecule. By reorienting upon transition, the o-H_2 also makes a transition.[13] This simultaneous transition is sometimes represented with the notation $Q_v(0)+Q_0(1)$, but will be herein referred to simply as the $Q_v(0)$ transition.

The $Q_v(0)$ transitions can also be induced by a laser field (stimulated Raman effect) or by an external electric field (Condon effect) in pure parahydrogen crystals. There are, however, qualitative differences between the impurity induced $Q_v(0)$ transitions and these Raman-type field-induced ones. The field-induced $Q_1(0)$ Raman transition in a pure parahydrogen crystal, obeys the exciton momentum selection rule $\Delta\mathbf{k}=0^+$, which arises from the translational symmetry of the crystal. Since all lattice sites have the same transition energy, the matrix element may then be factored out of the crystal sum, leaving a δ function for $\mathbf{k}=0^+$.[3] These transitions are thus observed to exhibit very narrow linewidths on the order of 10 MHz [half width at half maximum (HWHM)].[14] The impurity-induced $Q_1(0)$ infrared transition, however, is much broader. As a result of the absorption mechanism, the o-H_2 destroys the translational symmetry of the p-H_2 lattice, and hence the $\Delta\mathbf{k}=0$ exciton momentum selection rule is disobeyed. This makes all states of the vibrational energy band infrared active and a line profile similar to the calculated density of vibron Bloch states is observed for the $Q_1(0)$ transition.[15] This $4\,\mathrm{cm}^{-1}$-wide band obscures all information about the o-H_2/p-H_2 interaction facilitating the absorption. The theoretical density of states calculated by Bose and Poll[15] agrees well with the observed $Q_1(0)$ infrared spectrum.

The infrared-active $Q_2(0)$ transition has also been observed, but under low resolution by both Lee[7] and Patel *et al.*[16] Observed with a medium resolution Fourier transform infrared spectrometer, the $Q_2(0)$ appears as two peaks separated by $0.33\,\mathrm{cm}^{-1}$.[17,18] Recently Momose *et al.* observed that the two peaks can be further resolved into many sharp spectral lines using an infrared laser spectrometer.[19]

The $Q_3(0)$ transitions appear as sharp spectral lines, and high-resolution laser spectroscopic techniques may be fully exploited for its study. The extremely narrow linewidths in solid hydrogen spectroscopy were first demonstrated in the microwave work of Hardy, Berlinsky, and Harris,[20] and the corresponding infrared work on o-H_2 impurity pairs in solid parahydrogen by Chan *et al.*[21] Recently, it was found that solid parahydrogen exhibits very narrow transitions that can be more than two orders of magnitude narrower than those in the gas phase. Since this initial high-resolution infrared observation, we have gained much insight into the nature of these solid state interactions.

The analysis of the fine structure of the $Q_3(0)$ transition lines has been greatly facilitated by the study of isotopic impurities (o-D_2, p-D_2, and HD) by Weliky *et al.* who observed the orthohydrogen-induced vibrational transitions of $J=0$ isotopic impurities in the solid parahydrogen matrix. These transitions occur by a mechanism similar to that of the parahydrogen $Q_1(0)$ transition, but they are much sharper.[18,22] Since these are impurity transitions, no exciton bands exist, and the nature of the intermolecular interaction can be elucidated more readily. Due to the localization of the vibrational energy on the HD or D_2 molecule, these transitions appear as several very sharp [approximately 5 MHz (HWHM)] main lines with many satellites. The ground and excited state splittings due to the isotopic impurity $J=0/J=1$ pair have been elucidated from the whole series of lines that have been assigned to specific quantum states of these matrix isolated impurity pairs.[18,22] The field-induced Raman line of this transition appears near the center of gravity of all lines,[18] with a linewidth seemingly limited by the crystal quality or $J=1$ and isotopic impurity broadening. These impurity data give a glimpse of the important interactions in hydrogenic vibrational transitions which, until now, have been obscured in transitions of the host molecules.

II. EXPERIMENT

The solid parahydrogen sample preparation is as previously described.[23,24] Hydrogen gas (Midwest Welding Supply Company) is first purified by passing it through a palladium film (Johnson-Mathey hydrogen purifier) to remove any nonhydrogenic impurities; it was then converted to the desired para-H_2 concentration (98%, 99.6%, 99.8%, 99.9%, or 99.95%) by passing the gas over a paramagnetic nickel silicate catalyst[25] at liquid hydrogen temperatures. In order to obtain a parahydrogen crystal purer than 99.8%, the conversion temperature must be kept below 20 K. This is performed by cooling with the vapor just above liquid He, or by pumping on the liquid H_2 bath cooling the catalyst. The converted gas was flowed into an 11.5 cm copper cell with wedged sapphire windows and frozen onto the cell walls. The dewar housing the cell was constructed by Infrared Laboratories, Inc. The hydrogen gas was flowed into the cell at a rate that maintained the liquid helium-cooled cell at approximately 7 K. Crystals formed in this manner are optically transparent and largely free of cracks, but the center of the cell usually remains empty. The laser radiation was passed near the wall where the full length of 11.5 cm is filled with the crystal with its c axis perpendicular to the surface of the wall.

Pumped by a Coherent Innova 100 argon-ion laser, a Coherent Model 899-29 titanium sapphire ring laser provides tunable near-infrared radiation that was passed through solid parahydrogen crystals with various concentrations of orthohydrogen impurity. Absorptions were detected by the change in intensity of the chopper-modulated laser after several passes through the sample. For lower $J=1$ concentration crystals only one pass through the sample was employed so the polarization dependence could be observed and toneburst modulation, yielding a second derivative line shape, was used to obtain a sensitivity of 3×10^{-5} $(\Delta I/I)$. The tone

frequency was varied from 100 to 15 MHz, thus generating sidebands on the laser frequency ν_o at $\nu_o \pm \nu_{\text{tone}}$. The burst frequency amplitude modulated the sidebands between 0 and 30% of the carrier intensity; this frequency was approximately 30 kHz. One beam passing through the crystal and one beam split before the crystal were either ratioed or subtracted to normalize the signal, thus reducing noise due to laser power fluctuations.

The titanium sapphire laser ($Ti:Al_2O_3$) is frequency stabilized to 500 kHz (rms) by an external 1 GHz Fabry-Perot cavity. The scanning can be performed manually over a 30 GHz ($1\ cm^{-1}$) range, or the laser can be controlled by the computer and Coherent's Autoscan program. The system scans by piecing together 10 GHz segments for any frequency range desired. The computer reads the wavemeter, thus giving an absolute frequency measurement good to seven digits. For a finer frequency measurement, iodine reference lines are collected simultaneously whose measured frequencies are published.[26] A 2 GHz spectrum analyzer is then used as an etalon to give reference marks, thus dividing up the 30 GHz scan into 15 smaller 2 GHz sections. These reference ticks, with the iodine lines, then allow for absolute frequency measurements with accuracy to eight significant digits. Since all the iodine transitions in this frequency range are hot bands, the cell is heated to 600 °C. The published data between 11 000 and 13 000 cm^{-1} were recorded at 700 °C; therefore, the intensities of these reference lines should not be relied upon when comparing with the literature. The data were collected simultaneously by the computer and a chart recorder. The polarization dependence of this transition was also checked by inserting a half wave plate followed by a polarizer to insure that the radiation was plane polarized. Both polarizations, parallel and perpendicular to the crystal axis, were checked with one pass through the crystal.

III. OBSERVED SPECTRUM

The $Q_3(0)$ transition has been observed in many different parahydrogen crystals with impurity o-H_2 concentrations of 2%, 0.45%, 0.2%, 0.12%, 0.095%, and 0.05%. The linewidths and intensities of the spectra vary greatly with impurity concentration. Since this is an impurity-induced transition, the integrated intensity is proportional to the o-H_2 concentration. The multipole fields and symmetry-breaking properties of the o-H_2 molecules, however, make the spectral lines broader at higher impurity concentrations. The $Q_3(0)$ transition of p-H_2 was initially observed in a crystal with 2.0% o-H_2 using chopper modulation and four passes through the crystal yielding a 40 cm path length.[18] The sensitivity using chopper modulation was $\Delta I/I \sim 7\times10^{-3}$. As the o-H_2 concentration was reduced, the $Q_3(0)$ transition was only observable with higher sensitivity techniques. Toneburst modulation (yielding a second derivative line shape) with noise subtraction and only one pass through the crystal was employed with a sensitivity of 3×10^{-5} in order to observe the weaker and narrower lines in the crystals with very low impurity concentrations. A signal-to-noise ratio of 300 was obtained with 65 MHz sidebands switched on and off at 30 kHz and detected using a 0.3 second time constant in the 0.095% o-H_2 crystal. Spectra recorded in several of these crystals are compared in Fig. 1. New features that had been obscured by inhomogeneous broadening became evident in the higher purity crystals. Strong polarization dependences have also been observed. The bottom spectrum in Fig. 1 shows the intensities of the peaks in the 0.095% $J=1$ crystal for incident radiation parallel to the crystal axis.

FIG. 1. Dependence of the $Q_3(0)$ spectrum on orthohydrogen impurity concentration. The top spectrum was recorded with a total pathlength of 40 cm and 2% orthohydrogen impurity; chopper modulation yields two peaks of approximately 400 MHz hwhm. The middle spectrum was obtained in a 0.5% impurity crystal with toneburst modulation (yielding second derivative line shapes), while the bottom toneburst modulated spectrum was obtained in a 0.095% impurity crystal.

A. Sharpness of the spectrum

Although the second overtone $Q_3(0)$ transition in solid parahydrogen is a factor of approximately 5600 weaker than the fundamental,[7] it is much narrower than the fundamental $Q_1(0)$ transition which is approximately $4\ cm^{-1}$ in its total extent. The large bandwidth in the latter transition is a result of the vibrational coupling among the parahydrogen molecules. For higher vibrational excitation, the coupling is weaker and the vibrational energy is increasingly localized on the absorbing molecule. Because the large anharmonicity in the vibrational energy spacing [$\omega_e x_e = 121.34\ cm^{-1}$, where $\omega_e x_e$ is the coefficient of $(v+\frac{1}{2})^2$ in the power series expansion of vibrational energy] causes a large mismatch between the hot band transitions and the fundamental, the $Q_3(0)$ vibron cannot split into 3 $Q_1(0)$ vibrons, but must remain as one $Q_3(0)$ vibron. The hopping is effected through the dispersion potential energy between two hydrogen molecules, V_{disp}, which can be expanded as

$$\hat{V}_{\text{disp}}(q_1,q_2) = \sum \frac{1}{m!n!}\left[\frac{\partial^{m+n} V_{\text{disp}}}{\partial q_1^m \partial q_2^n}\right] q_1^m q_2^n, \qquad (1)$$

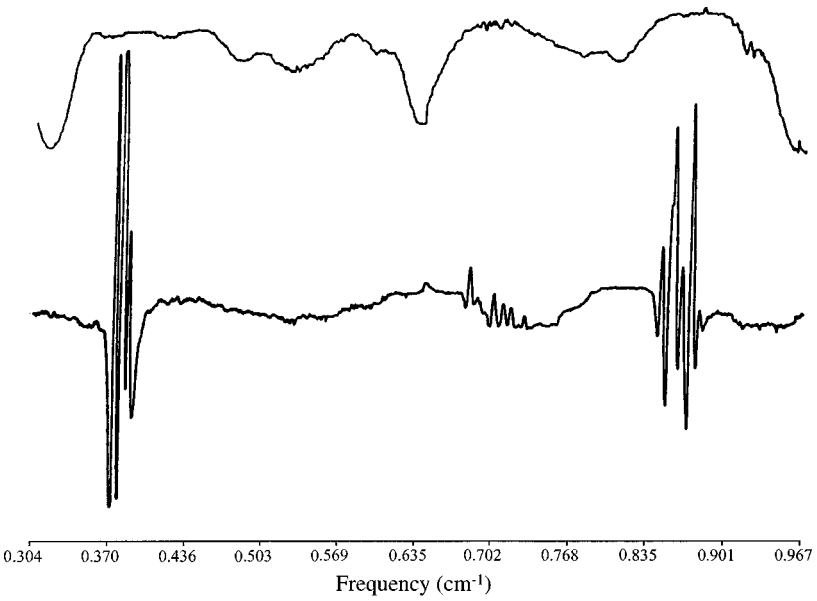

FIG. 2. $Q_3(0)$ spectrum of solid parahydrogen: parallel polarization. This spectrum was taken in a 0.095% impurity crystal and shows 17 transitions. The highest and lowest frequency transitions have overloaded the lock-in amplifier. 11 758.000 cm^{-1} should be added to the numbers shown in the bottom to obtain wave numbers of spectral lines.

where q_1 and q_2 are the vibrational coordinates of hydrogen molecules 1 and 2, respectively. For convenience we take dimensionless vibrational coordinates such that

$$\langle v|q^2|v\rangle = v + \tfrac{1}{2} \quad \text{and} \quad \langle v|q|v-1\rangle = \sqrt{v/2}.$$

From a general principle for such an expansion, the orders of magnitude of the coefficients are

$$\frac{1}{m!n!}\left[\frac{\partial^{m+n}V_{\text{disp}}}{\partial q_1^m \partial q_2^n}\right] \sim \kappa^{m+n} V_{\text{disp}},$$

where $\kappa = \sqrt[4]{m_e/M} \approx 0.1$ is the Born-Oppenheimer constant with the electron mass m_e and the nuclear mass M. The hopping of the $Q_v(0)$ vibron is effected by the term $(q_1 q_2)^v$ in Eq. (1) through the matrix element

$$\langle v_1 = v, v_2 = 0|\hat{V}_{\text{disp}}|v_1 = 0, v_2 = v\rangle = \frac{1}{2^v}\frac{1}{v!}\frac{\partial^{2v}V_{\text{disp}}}{\partial q_1^v \partial q_2^v} \approx \frac{v!}{2^v}\kappa^{2v}V_{\text{disp}}.$$

We thus see that the vibron hopping frequency is reduced by two orders of magnitude as v increases by one.[27] This rough order of magnitude argument indicates that the $Q_2(0)$ transition has a hopping frequency of $\approx 0.04\ cm^{-1}$ (1.2 GHz), while that of the $Q_3(0)$ transition should be on the order of $0.0004\ cm^{-1}$ (12 MHz). This spectral sharpness is seen in the observed $Q_3(0)$ spectrum (Fig. 2) and has allowed us to assign the observed features to transitions between the individual quantum states of the $J=1/J=0$ pair of molecules. The strong low- and high-frequency transitions are shown on an expanded scale in Figs. 3 and 4, respectively, while the weak central features are presented in Fig. 5.

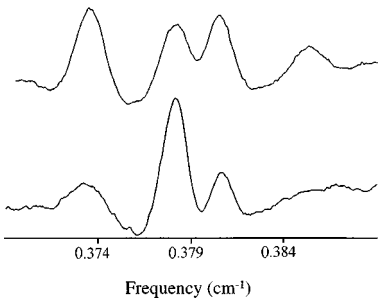

FIG. 3. Lowest frequency nearest-neighbor $Q_3(0)$ transitions. These are to the $J=1$, $M=0$ pair state. Four transitions are observed due to the difference of ip (peaks 2 and 4 in order of increasing frequency from left to right) and op (peaks 1 and 3) nearest-neighbor pairs. The ground-state crystal-field splitting of $0.0071\ cm^{-1}$ is clearly observed. Parallel and perpendicular polarizations of the laser relative to the crystalline axis are used for the upper and lower traces, respectively.

B. Field-induced spectrum

In addition to the o-H_2 induced $Q_3(0)$ transitions shown in Fig. 2, we have previously observed the electric field-induced $Q_3(0)$ transition in a 0.8 cm-long parahydrogen crystal with 0.2% o-H_2 impurity.[18,28] The field-induced transition is very weak since the transition dipole moment induced by the electric field (50 kV/cm) is only on the order of 3.35×10^{-7} D. The high sensitivity of the Condon modulation method ($\Delta I/I \approx 5\times10^{-6}$), however, has allowed us to observe the transition with a sufficient signal to noise ratio.[18] Unlike the $J=1$ H_2 induced spectrum that exhibits fine structure due to the simultaneous transitions of the $J=1$ H_2, the

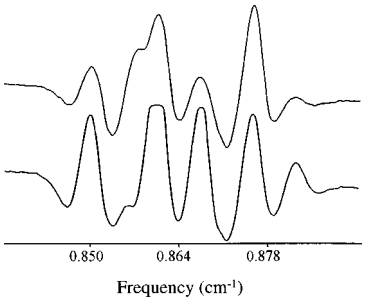

FIG. 4. Highest frequency transitions of the $Q_3(0)$ spectrum. These are to the $J=1$, $M=1\pm$ pair levels for both ip and op nearest neighbors. Parallel and perpendicular polarizations of the laser relative to the crystalline axis are used for the upper and lower traces, respectively. Two central components are saturated in the lower trace.

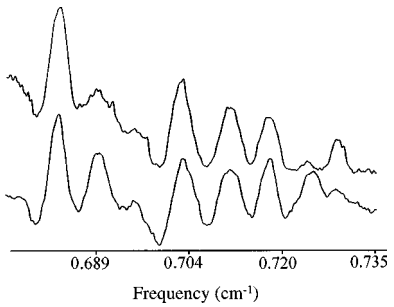

FIG. 5. Vibrational transitions due to more distant neighbors. The six lowest frequency transitions are due to next-nearest-neighbor induction, while the peak at 11 758.729 cm^{-1} is the Raman-active transition arising from the fields of all impurities far away, piling up at the field-induced transition frequency due to the $\Delta k=0$ selection rule.

field-induced spectrum appears as a single line, its frequency being very useful to locate the center of the $Q_3(0)$ transition. Since the external electric field induces dipole moments in the crystal, the crystalline translational symmetry is retained and the $\Delta\mathbf{k}=0^+$ exciton momentum selection rule applies to this transition. This selection rule, however, does not help to narrow the spectral line as it does in the Raman-active $Q_1(0)$ transition because the $Q_3(0)$ bandwidth is already very small due to the very low vibron hopping frequency discussed in Sec. III A, above.

Just like in the cases of the D_2 and HD impurity $Q_1(0)$ spectra, the field-induced $Q_3(0)$ transition appeared between the two widely split groups of lines; the spacings between the field-induced spectrum and the higher frequency group and that with the lower frequency group were approximately 1:2. This clearly indicates that the major splitting of ≈ 0.5 cm^{-1} in the $J=1$ induced $Q_3(0)$ transition (see Fig. 2) is due to the splitting between $M=0$ and $M=\pm 1$ sublevels in the excited vibrational state. It will be shown (shortly) that the magnetic quantum number M is defined with respect to the pair axis and to the crystal axis for the excited and ground states, respectively. The smaller splittings in each group of lines are due to a small splitting between $M=0$ and $M=\pm 1$ sublevels in the ground state, small splittings between $M=\pm 1$ levels in the excited state, as well as due to small energy differences between two inequivalent pairs, one in which the $J=1$ H_2 and the excited $J=0$ H_2 are in the same hexagonal plane and the other in which they are in different hexagonal planes. These spectral structures reflect the intricate interactions between the molecules and the crystal field. In particular, we have been able to determine the crystal-field splitting of the $J=1$ M sublevels directly.[29] This is in contrast to the case of the fundamental $Q_1(0)$ transition in which the large vibron band obscures these intricate structures.

C. Transition mechanism

The $Q_3(0)$ transition shown in Fig. 2 is induced by the same mechanism active in the $Q_1(0)$ transition that was initially worked out by Sears and VanKranendonk.[13] The quadrupole field of an impurity $J=1$ H_2 (molecule 1) induces dipole moments in the surrounding $J=0$ p-H_2 (molecule i) which is expressed in operator form as

$$\mu_m=\sqrt{35}\,\frac{\alpha Q}{R^4}\sum_n C(231;n,m-n)C_{2,n}(\Omega_1)C_{3,m-n}(\Omega_{1i}), \tag{2}$$

where Q is the electric quadrupole moment of molecule 1, α is the isotropic polarizability of molecule i, R is the distance between molecules 1 and i, Ω_1 and Ω_{1i} are the angular orientations of molecule 1 and the 1-i pair axis with respect to the crystalline c axis, respectively, $C(231;n,m\text{-}n)$ is a Clebsch-Gordan coefficient and $C_{2n}(\Omega_1)$ and $C_{3,m\text{-}n}(\Omega_{1i})$ are Racah spherical harmonics. The suffix m on the dipole moment μ indicates the spherical components of the dipole moment. For $m=0$, we observe parallel transitions while for $m=\pm 1$, perpendicular transitions. The crystal-fixed dipole operator of Eq. (2) induces the $Q_3(0)$ transition in one of the surrounding molecules i, molecule 2, through a transition dipole moment

$$\begin{aligned}\langle v_1=0,1M',v_2=3,0|\mu_m|v_1=0,1M,v_2=0,0\rangle \\ =\sqrt{35}\,\frac{\langle 0|Q|0\rangle\langle 3|\alpha|0\rangle}{R_{12}^4}\sum_n C(231;n,m\text{-}n) \\ \times\langle 1M'|C_{2,n}(\Omega_1)|1M\rangle C_{3,m\text{-}n}(\Omega_{12}),\end{aligned} \tag{3}$$

where $\langle 3|\alpha|0\rangle$ is the vibrationally off-diagonal matrix element of the isotropic polarizability theoretically calculated to be 1.5×10^{-3} $Å^3$. This value is three orders of magnitude less than that of the isotropic polarizability of 0.802 $Å^3$.[30] Equation (3) demonstrates that molecule 1 which induces the $Q_3(0)$ transition in molecule 2, simultaneously makes an orientational transition $1M'\leftarrow 1M$. It is this simultaneous orientational transition that produces the structure in the observed spectrum. Note that the excited state wave function $\langle 1M'|$, where M' is defined with respect to the pair axis, is a linear combination of $\langle 1M|$ where M is defined with respect to the crystal axis.

In the ground state the $J=1$ molecule is completely surrounded by $J=0$ H_2 molecules and the system retains its D_{3h} symmetry. Under such symmetry the $M=\pm 1$ levels are degenerate and the splitting between the $M=0$ and $M=\pm 1$ levels is very small due to the cancellation of the splitting interactions among nearest- and next-nearest-neighbors (the cancellation effect).[3,31] When one of the surrounding molecules is excited to the $v=3$ state, however, the D_{3h} symmetry is broken; the splitting between the $M=0$ and ± 1 levels is greatly amplified from less than 0.01 cm^{-1} to approximately 0.5 cm^{-1} and the degeneracy of the ± 1 levels is lifted. Moreover, the axis of approximate cylindrical symmetry changes from the crystal c axis to the pair axis, i.e., the axis between the $J=1$ H_2 and the excited $J=0$ H_2, and it is more convenient to take the M quantum number with respect to this pair axis rather than to the crystal axis. This variation of axis upon vibrational excitation introduces an additional complication which did not exist in the D_2 and HD impurity spectra in which the D_{3h} symmetry is broken in both the excited and the ground states. It should be noted that in our calculated intensities and assignments the M quantum numbers for the crystal axis and for the pair axis have been used for the ground and excited vibrational states, respectively. Although the $M=\pm 1$ degeneracy is lifted in the excited state, there remains a plane of symmetry that is the hexago-

nal plane for ip pairs and the plane formed by the pair axis and the c axis for op pairs. The two $M=\pm 1$ levels are therefore expressed by the two pair frame states that are symmetric or antisymmetric with respect to this plane:

$$|11\pm\rangle=[|11\rangle\pm|1-1\rangle]/\sqrt{2}. \quad (4)$$

IV. ANALYSIS OF OBSERVED SPLITTINGS

The angle-dependent intermolecular interactions underlying the observed intricate structure of the $Q_3(0)$ transition can be treated as a sum of pairwise intermolecular interactions. The most general form of the pairwise interaction is[3]

$$A(R,\omega_1,\omega_2)=\sum_{l_1,l_2,m} A_{l_1 l_2 m}(R)C_{l_1 m}(\omega_1)C_{l_2 \bar{m}}(\omega_2), \quad (5)$$

where ω_1 and ω_2 are angle variables with respect to the pair axis and R is the intermolecular distance. For the calculation of the simple system in which molecule 1 has $J=1$ and molecule 2 $J=0$, however, it suffices to consider only terms with $l_1\leqslant 2$ and $l_2=0$ since other terms do not have nonvanishing matrix elements. Since $l_1=1$ vanishes from the symmetry of H_2, the only angle-dependent term that should be considered in the manifold of the $J=1$ and $J=0$ pair is

$$A(R,\omega)=B(R)C_{20}(\omega), \quad (6)$$

where ω is the angular variable for $J=1$ H_2. The total angle-dependent interaction between the $J=1$ H_2 and the surrounding $J=0$ H_2 is given by a sum

$$V(\Omega)=\sum_{\rho=2}^{N} A(R_\rho,\omega_\rho)=\sum_{\rho=2}^{N} B(R_\rho)C_{20}(\omega_\rho)$$
$$=\sum_{\rho=2}^{N} B(R_\rho)\sum_{m=-2}^{2} C_{2m}(\Omega)C_{2m}^{*}(\Omega_\rho), \quad (7)$$

where ρ specifies the relative positions of $J=0$ molecules with respect to the $J=1$ molecule and Ω and Ω_ρ are the crystal-fixed angle variables of the $J=1$ H_2 and the vector R_ρ, respectively.

The potential $V(\Omega)$ is simplified for the lower state of the $Q_3(0)$ transition to

$$V(\Omega)=\varepsilon_{2c}C_{20}(\Omega) \quad (8)$$

since the crystal sum over ρ,

$$\varepsilon_{2c}\equiv\sum_{\rho=2}^{N} B(R_\rho)C_{20}(\Omega_\rho), \quad (9)$$

is nonvanishing only for $m=0$ due to the D_{3h} symmetry. This term gives the crystal-field splitting in the ground state between the $M=\pm 1$ level and the $M=0$ level to be

$$\Delta=E(M\pm 1)-E(M=0)=-0.6\varepsilon_{2c}. \quad (10)$$

It is known that the cancellation effect in the summation (9) for nearest-neighbor and next-nearest-neighbor interactions makes the value of ε_{2c}, and thus Δ, very small.[3]

For the excited state, $V(\Omega)$ is more complicated since the value of $B(R_2^*)$ for the excited molecule 2 is different from $B(R_\rho)$ in the ground state and thus the D_{3h} symmetry is broken. In this case we can write

$$V(\Omega)=\varepsilon_{2c}C_{20}(\Omega)+[B(R^*)-B(R)]$$
$$\times\sum_{m=-2}^{2} C_{2m}(\Omega)C_{2m}^{*}(\Omega_\rho). \quad (11)$$

Since $\Delta B=B(R_2^*)-B(R_2)\approx 0.8\ \mathrm{cm}^{-1}$ is much larger than $\varepsilon_{2c}\approx 0.01$, **J** is quantized more along the pair axis rather than the crystal axis and it is more convenient to write

$$V(\omega)=\varepsilon_{2c}\sum_{m=-2}^{2} C_{2m}(\omega)C_{2m}^{*}(\omega_2)+\Delta B C_{20}(\omega), \quad (12)$$

where ω is the angular variable with respect to the pair axis and ω_2 is the angular variable of the crystalline c axis with respect to the pair axis. Thus the $M=\pm 1$ and $M=0$ levels with respect to the pair axis are separated by approximately $-0.6\Delta B$ by the second term of Eq. (12) and the first term removes the degeneracy of the $M=\pm 1$ levels. The more detailed eigenvalues of Eq. (12) in the manifold of the $J=1$ and $J=0$ pair are easily obtained as the solution of linear and quadratic equations as shown by Weliky *et al.*[22] Because the dispersion and induction interactions are linearly dependent on the molecular polarizabilities,[32] by employing the Hamiltonian presented in Eq. (12), the *ab initio* potential for hydrogen pairs given by Mulder and co-workers,[33] and the variation of the polarizability upon vibrational excitation given by Kolos and Wolniewicz,[30] we were able to calculate the approximate spectral pattern for the assignment of the fine structure.

Spectral assignment

The $Q_3(0)$ spectrum is enriched by the fact that two distinct types of nearest-neighbor pairs exist in the hcp lattice. The hcp lattice consists of hexagonal planes stacked $ababab\ldots$. This makes in-plane and out-of-plane pairs inequivalent. These therefore exhibit different splittings and intensities. The ground state, however, is identical for all sets of transitions (in plane, out of plane, and farther apart neighbors) because before any molecule absorbs radiation, the system merely consists of a $J=1$ hydrogen isolated in a parahydrogen crystal. Spectral intensities $|\mu|^2$ calculated by using Eqs. (3) and (4) are summarized in Fig. 6 for both (ip) and (op) nearest-neighbor pairs. The intensity calculation neglects the small mixing of M due to ε_{2c} in the excited state but it gives a good approximation since $\Delta B\gg\varepsilon_{2c}$. Based on these relative intensities, the intensity dependence on laser polarization, and the calculated splittings resulting from our anisotropic dispersion calculations, we have assigned all of the observed spectral features of the $Q_3(0)$ transition as listed in Table I. The accurately measured frequencies in Table I give a precise value of the $M=0$ and $M=\pm 1$ ground-state splitting that had been studied extensively both experimentally and theoretically over many years.[29] There are altogether eight pairs of transitions in our observed $Q_3(0)$ spectrum that give ground-state splittings ranging from 0.0070 to 0.0073 cm^{-1} with an average of 0.0071 $\pm 0.0002\ \mathrm{cm}^{-1}$.

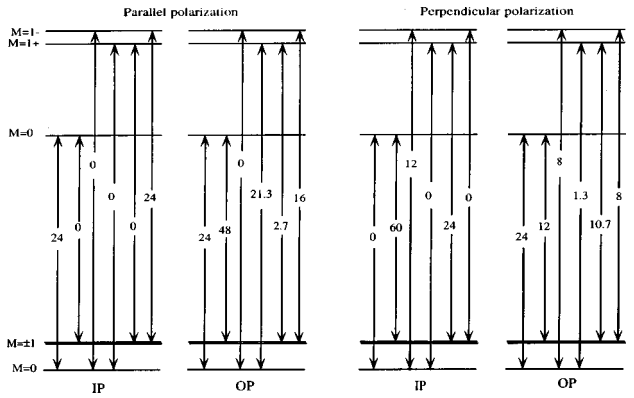

FIG. 6. Calculated $Q_3(0)$ relative intensities for nearest-neighbor pairs for parallel and perpendicular polarizations.

Because the polarization of the laser relative to the crystalline axis was not perfectly controlled due to optical imperfections of the windows and the crystal, only approximate agreement in polarization dependences were observed. Although the relative intensities and spacing of spectral lines were well reproduced in different samples, the absolute frequencies differ by up to 0.01 cm^{-1} between different crystals due to differing orthohydrogen concentration. Experimental frequencies and spectra for assignment are presented for the 0.095% impurity concentration crystal. The lower frequency quartet is most readily assigned. The ground-state splitting of 0.0071 ± 0.0002 cm^{-1} can be readily seen in this symmetric quartet. This is the first direct observation of this crystal-field splitting, and it agrees with the less direct NMR measurement of 0.0058 ± 0.003 cm^{-1} within the quoted uncertainty, which did not determine the relative ordering of the states.[34] The second and fourth lowest frequency peaks show the largest intensity changes with polarization. The peak at 11758.3776 cm^{-1} is the most intense peak in the spectrum and increases in perpendicular polarization while the much weaker transition at 11758.3846 cm^{-1} shows the opposite polarization dependence. Comparison with the calculated intensities indicates that these are the two in-plane transitions to the $|10\rangle$ state, while the remaining two transitions are the transitions to the out-of-plane excited state pair. The higher energy ensemble (Fig. 4) of peaks also exhibits the ground-state crystal-field splitting of the isolated o-H_2 molecule. This allowed us to identify pairs of transition ending up in the same excited state. Comparison with the calculated polarization dependences then yield the assignment given in Table I and the nearest-neighbor energy level diagram given in Fig. 7. Since six transitions are observed, and seven are expected, we have assigned two transitions to the one strong line that shows no polarization dependence at 11 758.8598 cm^{-1}. This seventh transition corresponds to an in-plane $|11-\rangle \leftarrow |11+\rangle$ transition and has no corresponding transition 0.0071 cm^{-1} higher in frequency because $|11-\rangle \leftarrow |10\rangle$ has no transition moment for both polarizations (see Fig. 7). The assigned spectral lines were fit to the pattern expected from Eqs. (8) and (12). The determined values of ΔB and ε_{2c} are listed in Table II.

TABLE I. Spectral assignment and frequencies of observed $Q_3(0)$ transitions.

Observed frequencies (in cm^{-1})	Assignment	
	Excited state pair type	$\lvert J'M'\rangle \leftarrow \lvert JM\rangle$
11 758.3731	out of plane	$\lvert 10\rangle \leftarrow \lvert 1\pm 1\rangle$
11 758.3776	in plane	$\lvert 10\rangle \leftarrow \lvert 1\pm 1\rangle$
11 758.3801	out of plane	$\lvert 10\rangle \leftarrow \lvert 10\rangle$
11 758.3846	in plane	$\lvert 10\rangle \leftarrow \lvert 10\rangle$
11 758.6817	next-nearest neighbor	$\lvert 10\rangle \leftarrow \lvert 1\pm 1\rangle$
11 758.6887	next-nearest neighbor	$\lvert 10\rangle \leftarrow \lvert 10\rangle$
11 758.7033	next-nearest neighbor	$\lvert 11-\rangle \leftarrow \lvert 1\pm 1\rangle$
11 758.7106	next-nearest neighbor	$\lvert 11-\rangle \leftarrow \lvert 10\rangle$
11 758.7173	next-nearest neighbor	$\lvert 11+\rangle \leftarrow \lvert 1\pm 1\rangle$
11 758.7245	next-nearest neighbor	$\lvert 11+\rangle \leftarrow \lvert 10\rangle$
11 758.7290	sum of more distant neighbors' fields	Raman transition $\lvert 00\rangle \leftarrow \lvert 00\rangle$
11 758.8492	out of plane	$\lvert 11+\rangle \leftarrow \lvert 1\pm 1\rangle$
11 758.8562	out of plane	$\lvert 11+\rangle \leftarrow \lvert 10\rangle$
11 758.8598	out of plane	$\lvert 11-\rangle \leftarrow \lvert 1\pm 1\rangle$(op)
	in plane	$\lvert 11+\rangle \leftarrow \lvert 1\pm 1\rangle$(ip)
11 758.8670	out of plane	$\lvert 11-\rangle \leftarrow \lvert 10\rangle$
11 758.8748	in plane	$\lvert 11-\rangle \leftarrow \lvert 1\pm 1\rangle$
11 758.8819	in plane	$\lvert 11-\rangle \leftarrow \lvert 10\rangle$

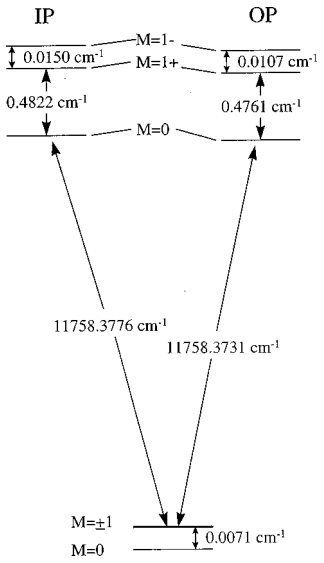

FIG. 7. Nearest-neighbor energy level diagram of the $Q_3(0)$ transition.

The origin of the ground- and excited-state splittings detailed in the previous section is confirmed experimentally by the set of weak lines near 11758.7 cm^{-1}. These are due to next-nearest-neighboring pairs undergoing the transition. All six next-nearest neighbors are equivalent lying out of plane

TABLE II. Experimentally derived $Q_3(0)$ crystal field and pair parameters.

Pair type	ΔB (cm^{-1})	ε_{2c} (cm^{-1})
ip nearest neighbors	−0.8037	+0.0250
op nearest neighbors	−0.7730	−0.0562
next-nearest neighbor	−0.0428	−0.0298
ground state	0	−0.0118

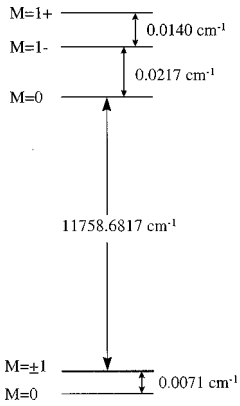

FIG. 8. Next-nearest-neighbor $Q_3(0)$ energy-level diagram.

and a distance of $R_0\sqrt{2}$ away. As expected, the ground-state crystal-field splitting of 0.0071 cm^{-1} is observed in this set of transitions as well. The intensities are expected to be weaker than the *nn*-induced transitions by a factor of $(R/R_0)^8 = 16$ and the splittings should be approximately 1/10th of the splittings of the main features based on Eq. (3) and our calculations employing the pair potential of Mulder *et al.*, respectively.[32] These weaker transitions scale approximately as expected both in intensity and in frequency, thus confirming that these transitions are indeed due to next-nearest neighbors of the o-H_2 molecule absorbing the vibrational energy. Assignments of these next-nearest-neighbor (NNN) transitions are also given in Table I while the energy level diagram is given in Fig. 8. From the intensity calculations for next-nearest neighbors, only six transitions are expected. Seven transitions are observed in this region, however. The seventh transition, appearing higher in frequency than all of the NNN induced transitions at 11 758.729 cm^{-1} is the field-induced transition reported previously.[18] This is due to all the $J=1$ o-H_2 that are located farther away than the next-nearest neighbors from the absorbing molecule adding up to give a nonzero dipole at the absorber. This transition, though weak, becomes weakly allowed and appears exactly at the Raman-active transition frequency. From Fig. 5 the field-induced transition frequency is seen to differ from the actual center of gravity of the observed infrared transitions. This is due to the shift of the infrared transition in the presence of the ortho-H_2 impurity. The frequency shift of the infrared transitions from the field-induced transition is readily explained by a linear extrapolation of the molar volume change between pure p-H_2 and pure o-H_2 crystals. Since the molar volume of solid o-H_2 is smaller than that of p-H_2, one expects the lattice to contract more or less homogeneously around the o-H_2 impurity, thus increasing the matrix shift of the infrared transitions to lower frequencies. As the center of the inducing field (here that of an orthohydrogen molecule) gets more distant from the absorbing molecule, the shift from the center, splittings, and intensities will get much smaller, and they will begin to pile up at the frequency of the Raman-active transition.

The first term in Eq. (12) is identical to Eq. (8) for the ground state of an isolated $J=1$ molecule. These parameters can be calculated directly from the experimental splittings, but the expressions differ for each type of neighboring pair undergoing the $Q_3(0)$ transition. While the ΔB term (pair interaction) is explained well by the change in polarizability, the crystalline interaction is not. Therefore, if our assumption in deriving Eq. (11) is valid, that is, if the vibrational excitation does not distort the crystal, the value of ε_{2c} determined from the observed spectrum using Eq. (11) should be identical to that of ε_{2c} for the ground state. The experimentally determined values of ε_{2c} listed in Table II clearly show that this is not the case and that the assumption made above is not valid. The small value of ε_{2c} is due to the well-known exact cancellation of the contribution from the nearest neighbors and the next-nearest neighbors in the crystal sum, Eq. (9). A small distortion of the crystal is sufficient to destroy the exact cancellation and cause the variation of ε_{2c}. This problem will be discussed separately in the following paper,[35] but the straightforward calculations presented in this paper do a good job of estimating the ground- and excited-state splittings and greatly aids the assignment by reinforcing the notion that the $M=0$ levels are lower in energy than are the $M=\pm 1$ levels.

V. CONCLUSIONS

As is shown in Fig. 2, ten main transitions have been observed in the $Q_3(0)$ spectrum, as well as seven smaller features falling near the center of gravity of these states. Based on the observed polarization dependences and our calculated splittings and intensities for this set of transitions, we have assigned these individual components of the $Q_3(0)$ transition to the different orientational components of the o-H_2 quadrupole field. The relevant quantities in determining both the selection rules and the frequency splittings are the p-H_2 polarizability and the position of the vibrationally excited molecule relative to the $J=1$ quadrupole moment. Since all of these transitions are dependent on angular interactions with the quadrupole moment of the $J=1$ molecule, in-plane and out-of-plane $J=1/J=0$ pairs have different M level energies in the crystal field. These differences manifest themselves as separate, resolvable transitions in the $Q_3(0)$ spectrum, and we have been able to directly observe the ground- and excited-state splittings due to both crystalline field and molecular pair interactions in the solid. Although the nature of these many-body interactions have only been alluded to in terms of a physical interpretation, the crystal-field parameter ε_{2c} seems to provide a sensitive probe of the underlying dynamics. This study has provided a rigorous quantum state assignment of all the levels involved in the parahydrogenic vibrational transition, and it is hoped that it will provide a basis for future theoretical investigations into solid-state interactions.

ACKNOWLEDGMENT

This work was supported by Air Force Grant No. F49620-94-1-0145.

*Present address: Department of Chemistry, Mail Code 0340, University of California at San Diego, 9500 Gilman Drive, La Jolla, CA 92093-0340.
†Present address: Department of Chemistry, Faculty of Science, Kyoto University, Kyoto, Japan.
‡Present address: Department of Chemistry, Auburn University, Auburn, AL 36849-5312.

[1] H. L. Welsh, in *MTP International Review of Science: Physical Chemistry Series One*, edited by A. D Buckingham and D. A. Ramsey (MTP Medical and Technical, Oxford, UK, 1972), Vol. 3, p. 33.
[2] E. U. Condon, Phys. Rev. **41**, 759 (1932).
[3] J. Van Kranendonk, *Solid Hydrogen* (Plenum, New York, 1983).
[4] T. Oka, Annu. Rev. Phys. Chem. **44**, 299 (1993).
[5] K. E. Kerr, T. Momose, D. P. Weliky, C. M. Gabrys, and T. Oka, Phys. Rev. Lett. **72**, 3957 (1994).
[6] J. VanKranendonk and G. Karl, Rev. Mod. Phys. **40**, 531 (1968).
[7] S. Y. Lee, Ph.D. thesis, The Ohio State University, 1987.
[8] E. Goovaerts, X. Y. Chen, A. Bouwen, and D. Schoemaker, Phys. Rev. Lett. **57**, 479 (1986).
[9] U. Buontempo, S. Cunsolo, P. Dore, and L. Nencini, Can. J. Phys. **60**, 1422 (1982).
[10] R. M. Dickson and T. Oka, J. Phys. C **99**, 2617 (1995).
[11] M. Okumura, M.-C. Chan, and T. Oka, Phys. Rev. Lett. **62**, 32 (1989).
[12] M.-C. Chan, S. S. Lee, M. Okumura, and T. Oka, J. Chem. Phys. **95**, 88 (1991).
[13] V. F. Sears and J. Van Kranendonk, Can. J. Phys. **42**, 980 (1964).
[14] T. Momose, D. P. Weliky, and T. Oka, J. Mol. Spectrosc. **153**, 760 (1992).
[15] S. K. Bose and J. D. Poll, Can. J. Phys. **65**, 67 (1987).
[16] C. K. N. Patel, E. T. Nelson, and R. J. Kerl, Phys. Rev. Lett. **47**, 1631 (1981); C.-Y. Kuo, M. M. F. Vieira, R. J. Kerl, and C. K. N. Patel, *ibid.* **50**, 256 (1983). I. Glatt, R. J. Kerl, C. K. N. Patel, *ibid.* **57**, 1437 (1986).
[17] M. Mengel, B. P. Winnewisser, and M. Winnewisser, Phys. Rev. B **55**, 10 420 (1997).
[18] D. P. Weliky, T. J. Byers, K. E. Kerr, T. Momose, R. M. Dickson, and T. Oka, Appl. Phys. B: Lasers Opt. **59**, 265 (1994).
[19] T. Momose, T. Nakamura, M. Miki, T. Wakabayashi, and T. Shida (unpublished).
[20] W. N. Hardy, A. J. Berlinsky, and A. B. Harris, Can. J. Phys. **55**, 1150 (1977).
[21] M.-C. Chan, M. Okumura, C. M. Gabrys, L.-W. Xu, B. D. Rehfuss, and T. Oka, Phys. Rev. Lett. **66**, 2060 (1991).
[22] D. P. Weliky, K. E. Kerr, T. J. Byers, Y. Zhang, T. Momose, and T. Oka, J. Chem. Phys. **105**, 4461 (1996).
[23] M.-C. Chan, S. S. Lee, M. Okumura, and T. Oka, J. Chem. Phys. **95**, 88 (1991).
[24] M.-C. Chan, Ph.D. thesis, The University of Chicago, 1991.
[25] APACHI catalyst, manufactured by Houndry Division, Air Products Corp.
[26] S. Gerstenkorn, J. Verges, and J. Chevillard, *Atlas du spectre absorption de la molecule d'iode* (Laboratoire Aime Cotton, CNRS II, Paris, 1982).
[27] T. Oka, in *Frontiers in Laser Spectroscopy*; Proceedings of the International School of Physics ''Enrico Fermi,'' Course CXX, edited by T. W. Hansch and M. Inguscio (North-Holland, New York, 1994), pp. 61–87.
[28] K. E. Kerr, Ph.D. thesis, The University of Chicago, 1995.
[29] R. M. Dickson, T. J. Byers, and T. Oka, J. Low Temp. Phys. **102**, 241 (1996).
[30] W. Kolos and L. Wolniewicz, J. Chem. Phys. **46**, 1426 (1967).
[31] T. Nagamiya and H. Kisi, Busseiron Kenkyu **39**, 64 (1951).
[32] H. C. Longuet-Higgins, Intermolecular-Forces, Discuss. Faraday Soc. **40**, 7 (1965).
[33] F. Mulder, A. van der Avoird, and P. E. S. Wormer, Mol. Phys. **37**, 157 (1979).
[34] R. Schweizer, S. Washburn, and H. Meyer, J. Low Temp. Phys. **37**, 289 (1979).
[35] R. M. Dickson and T. Oka, following paper, Phys. Rev. B **57**, 950 (1997).